Carbohydrate Polymers 110 (2014) 53–61

Contents lists available at ScienceDirect

Carbohydrate Polymers

journal homepage: www.elsevier.com/locate/carbpol

Water barrier properties of starch films reinforced with cellulose nanocrystals obtained from sugarcane bagasse

Aníbal M. Slavutsky[a,*], María A. Bertuzzi[b]

[a] Agencia Nacional de Promoción Científica y Tecnológica (ANPCyT), CIUNSa, Universidad Nacional de Salta, Av. Bolivia 5150, A4408TVY Salta, Argentina
[b] Instituto de Investigaciones para la Industria Química (CONICET), CIUNSa, Facultad de Ingeniería, Universidad Nacional de Salta, Av. Bolivia 5150, A4408TVY Salta, Argentina

ARTICLE INFO

Article history:
Received 25 May 2013
Received in revised form 6 March 2014
Accepted 19 March 2014
Available online 28 March 2014

Keywords:
Starch/CNC film
Sorption isotherms
Water barrier properties
Permeability
Diffusivity

ABSTRACT

Water transport in edible films based on hydrophilic materials such as starch, is a complex phenomenon due to the strong interaction of sorbed water molecules with the polymeric structure. Cellulose nanocrystals (CNC) were obtained from sugarcane bagasse. Starch and starch/CNC films were formulated and their water barrier properties were studied. The measured film solubility, contact angle, and water sorption isotherm indicated that reinforced starch/CNC films have a lower affinity to water molecules than starch films. The effects that the driving force and the water activity (a_w) values at each side of the film have on permeability were analyzed. Permeability, diffusivity, and solubility coefficients indicated that the permeation process depends mostly on the tortuous pathway formed by the incorporation of CNC and therefore were mainly controlled by water diffusion. The interaction between CNC and starch chain is favoured by the chemical similarities of both molecules.

1. Introduction

Polysaccharides such as starch, cellulose derivates and plant gums have been studied as edible films and coatings in food packaging and preservation (Kester & Fennema, 1986). Generally, the main functional properties of these hydrophilic materials depend strongly on their water content and therefore on the surrounding humidity. The relationship between water activity (a_w) and the moisture content of a material is explained by means of its moisture sorption isotherms. Water permeability depends on its solubility and diffusivity, the former is obtained from water sorption isotherms while the latter is related to the diffusion path of water molecules in the film matrix. In addition, water also acts as a plasticizer for hydrophilic materials and a swelling process occurs affecting the barrier properties, which depend strongly on water content (Bertuzzi, Armada, & Gottifredi, 2003).

Nanotechnology focuses on the characterization, fabrication and manipulation of biological and nonbiological structures smaller than 100 nm. The design of internal micro or nanoscale structures can improve the functional properties, morphology and stability of the polymer matrix used in edible films and coatings (Azeredo, 2009). Cellulose is the most abundant renewable polymer in the world; it is found in plant cell walls, and it can also be synthesized by some bacteria. Its reinforcing property is remarkable (Tashiro & Kobayashi, 1991). Basically two types of nanoreinforcements can be obtained from cellulose: microfibrils and whiskers. In the case of plants or animals, the cellulose chains are synthesized to form microfibrils (or nanofibres), which are bundles of molecules that are elongated and stabilized through hydrogen bonding (Wang & Sain, 2007). The microfibrils have nanosized diameters (2–20 nm, depending on the origin), and their lengths are in the micrometre range (Azizi Samir, Alloin, Sanchez, & Dufresne, 2004; Oksman, Mathew, Bondeson, & Kvien, 2006). Each microfibril is formed by aggregation of elementary fibrils, which are made up of crystalline and amorphous parts. The crystalline parts, which can be isolated by several treatments, are the whiskers, also known as nanocrystals (CNC), nanorods, or rodlike cellulose microcrystals (Azizi Samir et al., 2004; Dujardin, Blaseby, & Mann, 2003), with lengths ranging from 500 nm up to 1–2 μm, and about 8–20 nm or less in diameter (Azizi Samir et al., 2004; Lima & Borsali, 2004), resulting in high aspect ratios. Each microfibril can be considered as a string of whiskers connected by amorphous domains (which act as structural defects), and having a modulus close to that of a crystal of native cellulose (about 150 GPa) and a strength of about 10 GPa

* Corresponding author at: Instituto de Investigaciones para la Industria Química (CONICET), CIUNSa, Universidad Nacional de Salta, Av. Bolivia 5150, A4408TVY Salta, Argentina. Tel.: +54 387 425541; fax: +54 387 4251006.
E-mail address: amslavutsky@gmail.com (A.M. Slavutsky).

http://dx.doi.org/10.1016/j.carbpol.2014.03.049
0144-8617/

(Helbert, Cavaillé, & Dufresne, 1996). These values are only about seven times lower than those of single walled carbon nanotubes (Podsiadlo et al., 2005).

Bagasse is the by-product obtained after sucrose extraction from the sugar cane plant. It has a high proportion of cellulose, which can be readily isolated from the other components namely lignin and hemicelluloses. The cellulose is obtained from bagasse by a pulping process (Zanin et al., 2000). Bondeson and Oksman (2007), Paralikar, Simonsen, and Lombardi (2008), Svagan, Hedenqvist, and Berglund (2009) and Belbekhouche et al. (2011) obtained nanocomposites based on different polymer matrices reinforced with cellulose fibres or whiskers. Kvien, Sugiyama, Votrubec, and Oksman (2007) and Savadekar and Mhaske (2012) studied the effect of CNC incorporation on thermoplastic starch matrix and found that the incorporation of nanofillers improved their barrier and mechanical properties.

The description and prediction of water vapour transport through hydrophilic films are extremely complex. The complexity is due to the nonlinear behaviour of water sorption isotherms and the water content dependency on diffusivity at high water activities. Water vapour transmission rate of hydrophilic films varies nonlinearly with water vapour pressure (Wiles, Vergano, Barron, Bunn, & Testin, 2000) at water activities higher than 0.55. At lower water activities, Wiles et al. (2000) and Debeaufort, Voilley, and Meares (1994) reported a linear dependence of water vapour transmission rate with water vapour pressure. Larotonda, Matsui, Sobral, and Laurindo (2005) and Müller, Yamashita, and Borges Laurindo (2008) investigated the influence of the diffusion coefficient (D_{eff}), the water vapour permeability (P) and the solubility coefficient of water (β) in different polymers. The β value, called film hydrophilicity, can be calculated from the first derivative of the water sorption isotherm (represented by GAB model fit) in relation to a_w, divided by the water vapour pressure (p_w) at the sorption isotherm temperature. The average β values for each range were determined and represented by β'. Water vapour permeability can be obtained using the ASTM E96 method (Bertuzzi, Castro Vidaurre, Armada, & Gottifredi, 2007). The diffusivity coefficient can be obtained from solubility and permeability coefficients (Larotonda et al., 2005).

The aim of this work was to determine the effect of variations of assay parameters such as water vapour gradient (permeation process driving force) and water vapour pressure values at each side of the film on water vapour permeability of starch/CNC nanocomposite films.

2. Materials and methods

2.1. Materials

Commercial and food grade corn starch (Unilever, Argentina) was used as the polymeric matrix for film formulation. Sugarcane bagasse was kindly supplied by Ingenío Río Grande (Jujuy, Argentina). Glycerol (Mallinckrodt, USA) was added as plasticizer. Ethylene glycol anhydrous (water content <0.003%) (Mallinckrodt, USA) was used for density determinations. P_2O_5 (Mallinckrodt, USA) was utilized as desiccant and saturated solution of $Mg(NO_3)_2$ (Mallinckrodt, USA) was used to obtain 53% RH. NaOH (Merk, Argentina) and $NaClO_2$ (Clorox, Argentina) were employed to obtain cellulose fibres. H_2SO_4 (Cicarelli, Argentina) was used in the acidic hydrolysis of cellulose fibres in order to obtain CNC. All salts used to achieve different relative humidity ambient (% RH) were provided by Aldrich (USA).

2.2. Preparation of CNC

Cellulose fibres (CF) were obtained by alkaline hydrolysis. 10 g of sugarcane bagasse were hydrolysed with 100 mL of NaOH (6%) at 60 °C for 4 h using a shaker. Next, the fibres were filtered to remove the excess of NaOH and washed with 200 mL of distillate water. Bleaching process consisted in the introduction of the material into a flask containing 200 mL of $NaClO_2$ (30%) and its shaking during 24 h at room temperature. After that, the fibres were filtered and washed with distilled water until neutral pH. The cellulose fibres were dried at 50 °C until constant weight. The cellulose, lignin and hemicelluloses contained in baggase were determined by means of the techniques proposed by Geoering and Van Soest (1970) using a Fibre Analyzer (ANKOM Technology Fiber Analyzer Model 220, USA). CNC were extracted from cellulose fibres, according to the methodology proposed by Bondeson, Mathew, and Oksman (2006). About 10 g of fibres were dispersed in 200 mL of H_2SO_4 (64%) into a flask under mechanical stirring. Hydrolysis was performed at 40 °C under vigorous stirring during 3 h. The excess of H_2SO_4 was removed from the resulting suspension by centrifugation at 800 rpm during 10 min. After that, the suspension was dialyzed against distilled water using a cellulose membrane until the pH reached 6–7. The resulting suspension was introduced into an ultrasonic bath for 1 h and stored in a refrigerator.

2.3. Film preparation

Film-forming solution was prepared by mixing starch (4%), glycerol (20% dry weight), water, and an appropriate amount of CNC suspension (prepared as was described in Section 2.2) in order to obtain a CNC concentration of 3% dry weight. The resulting dispersion was kept 60 min in an ultrasonic bath. Dispersions were gelatinized in a shaking water bath at 78–80 °C during 10 min. This procedure ensured disintegration of starch granules and formation of a homogeneous dispersion. The resulting dispersion, while still hot, was poured on polystyrene plates. Then, they were placed in an air-circulating oven at 35 °C and 53% RH for 15 h. After that, plates were removed from the oven and films were peeled off.

2.4. Characterization of CNC. Scanning electron microscopy (SEM), transmission electron microscopy (TEM) and X-ray diffraction (XRD)

CNC powder and cellulose fibres were analyzed. X-ray diffraction spectra were carried out in a diffractometer Rigaku Mini Flex (Japan), using a Cu kα radiation, 40 kV and 20 mA over an angular range 1–40° with step size 0.02. Samples were previously conditioned at a relative humidity of 53% and 25 °C.

CNC powder and cellulose fibres were examined by SEM utilizing a JEOL JSM 6480 LV scanning microscope. Samples were stored at 25 °C over silica gel. Powder samples were mounted on bronze stubs and coated with gold plasma. Samples were observed using an accelerating voltage of 20 kV.

An aliquot of CNC suspension was diluted and sonicated for 5 min (Branson 450 sonifier). A drop of this resultant diluted suspension was deposited on a carbon microgrid net (400 meshes) and the grid was stained with a 1.5% solution of uranyl acetate and dried at room temperature. Transmission electron micrographs (TEM) images were obtained using a JEOL JEM-1011 HR transmission electron microscope with an acceleration voltage of 80 kV.

2.5. Scanning electron microscopy (SEM) of starch/CNC films.

Cross-sections of starch/CNC films were examined by SEM using a JEOL JSM 6480 LV scanning microscope. For cross-section observations, films were cryofractured by immersion in liquid nitrogen.

Samples were stored at 25 °C over silica gel. Film samples were mounted on bronze stubs and coated with gold–palladium alloy. Samples were observed using an accelerating voltage of 20 kV.

2.6. Film solubility in water

Film solubility in water was measured as percentage of film dry matter solubilized in water during a period of 24 h. The initial dry matter of each film was obtained after drying film specimens in desiccators containing P_2O_5 during a week. Samples of approximately 100 mg were weighed and immersed in 20 mL distilled water at 30 °C, sealed and agitated. Film matrix not solubilized in water was separated by centrifugation (Sigma 4K10, Germany) at 2500 × *g* and dried at 40 °C to determine the remaining dry matter. Tests were performed by triplicate and solubility was calculated as follows:

$$\text{Solubility } (\%) = \frac{\text{initial dry weight} - \text{final dry weight}}{\text{initial dry weight}} \times 100 \quad (1)$$

2.7. Surface hydrophobicity assay

The objective of this analysis was to determine the hydrophobicity behaviour of starch and starch/CNC films. Surface hydrophobicity and contact angle (θ) measurements were performed by the sessile drop method at room temperature, using a goniometer (Standard Goniometer with DROP image standard, model 200-00, Ramé-Hart Instrument Co, Succasunna, USA). Surface hydrophobicity was evaluated in static contact angle experiments. A small water droplet was released on the film surface, digital pictures were gathered and the image produced by the software was used to calculate the formed angle. The contact angle measurements were performed at initial time. Five readings were taken on different parts of each film, the average of the contact angle values and the standard deviation were calculated.

The surface free energy (γ_S) was obtained from the surface equation of state:

$$\cos\theta + 1 = 2 \cdot \sqrt{\left(\frac{\gamma_S}{\gamma_L}\right) e^{-\beta \cdot (\gamma_L - \gamma_S)^2}} \quad (2)$$

where θ is the contact angle, γ_L is the surface tension of the liquid, and $\beta = 0.0001247\ m^2\ mN^{-2}$, is an experimentally determined parameter, proposed by Kwok and Neumann (1999) and obtained from the equipment user' manual. The programme uses an iterative process to solve Eq. (2). The relation needed for γ_S ($mJ\ m^{-2}$) calculation is given by Young's equation:

$$\gamma_S = \gamma_{SL} + \gamma_{SL} \cdot \cos\theta \quad (3)$$

where γ_{SL} ($mJ\ m^{-2}$) is the polymer–liquid interfacial energy and γ_L ($mJ\ m^{-2}$) is the surface tension of the liquid. The contact angle is usually measured by the tangent at the three phase interface (solid–liquid–vapour) (Kwok & Neumann, 1999).

2.8. Mechanical properties

The tensile properties were measured using a texturometer Brookfield (USA) according to ASTM D882 (2000) with some modifications. The films were cut into strips 25.4 mm wide and 80.0 mm long using a sharp scalpel. The final exposed film area was 25.4 mm × 50.0 mm. The texturometer was set to tensile mode. Initial grip separation was 50 mm. Force and elongation was recorded during extension at 20 mm/min up to break. Before tension assay, all film strips were equilibrated during a week in a cabinet conditioned at 25 °C and 52% relative humidity using saturated magnesium nitrate solution. Five samples of each film formulation were tested in order to determine the % elongation at break (% ε), tensile strength (T) and Young' modulus (Y).

2.9. Density

Film density was determined by pycnometry (displacement method). Due to the high solubility of starch films in water, ethylene glycol was used. The weak ethylene glycol/starch affinity ensures the non-penetration of ethylene glycol in the film matrix. The initial dry matter of each film was obtained after drying the film specimens in desiccators containing P_2O_5 during a week. Measurements were performed in triplicate. Density was calculated as follows:

$$\rho = \frac{m_p}{V_m} \quad (4)$$

where ρ is the density ($g\ cm^{-3}$), m_p (g) is the dry film weight and V_m (cm^3) is the film volume.

2.10. Determination of moisture sorption

Constant relative humidity environments were established inside sorbostats (glass jars), using salt solutions. The salts used (LiBr, LiCl, CH_3COOK, $MgCl_2$, K_2CO_3, $Mg(NO_3)_2$, NaBr, NaCl, KCl) were the different salts recommended by the European project COST-90 (Spiess & Wolf, 1983), to cover a water activity (a_w) range from 0.05 to 0.90. Film samples (rectangular strips of approximately 2 cm^2 area) were first freeze-dried (Thermovac Industries Corp., USA) and stored in a desiccator with P_2O_5 during 48 h. Samples were weighed and each one was placed on a plastic lattice by holding it on a tripod inside the sorbostats that contain the different saturated salt solutions. Then the sorbostats were sealed. The sorbostats were kept inside an environmental chamber maintained at constant temperature (25 °C). Film samples were equilibrated in the sorbostats for 4 days before their weights were recorded. The weights of the samples were checked during 3 more days. Equilibrium was judged to have been attained when the difference between two consecutive sample weightings was less than 1 mg/g dry solid. Data were reported for each relative humidity as gram of water sorbed/100 g dry film. The moisture sorption measurements were performed in quadruplicate at each a_w.

The data obtained were fitted by GAB sorption model, as described by Eq. (5):

$$w_e = \frac{w_0 \cdot C \cdot k \cdot a_w}{(1 - k \cdot a_w)(1 - k \cdot a_w + C \cdot k \cdot a_w)} \quad (5)$$

where w_e is the equilibrium moisture content (g water/100 g dry film), w_0 is the monolayer content (g water/100 g dry film), C is Guggenhein constant related to sorption heat monolayer, k is a correction factor related to sorption heat multilayer.

The quality of the fitting was evaluated through R^2 and through the mean relative percent error (% Error) defined as:

$$\%\,\text{Error} = \sum_{n=1}^{n} \left[\left| \frac{w_{e,i} - w_{p,i}}{w_{e,i}} \right| \right] \times \frac{100}{n} \quad (6)$$

where n is the number of data points, $w_{e,i}$ and $w_{p,i}$ are experimentally observed and predicted by the model values of the equilibrium moisture content, respectively. The percentage error (% Error) has been widely adopted throughout the literature to evaluate the goodness of fit of sorption models. A % Error value below 10% is indicative of a good fit for practical applications (Al-Muhtaseb, McMinn, & Magee, 2002).

2.11. Water vapour permeability

The apparatus and methodology described in the ASTM E96 (ASTM, 2000a,b) were used to measure film permeability. Film specimens were conditioned for 48 h in a chamber at 25 °C and 53% relative humidity ($Mg(NO_3)_2$ saturated salt solution) before

being analyzed. Films were sealed on cups containing different saturated salt solutions or distilled water that provides higher relative humidity. Test cups were placed in a desiccator cabinet maintained at constant temperature. Saturated salt solutions were used to provide specific relative humidity. In all cases, relative humidity inside the desiccator cabin was lower than relative humidity inside the cups. Table 4 shows the range of a_w used in each assay. A fan was used to maintain uniform conditions at all test locations over the specimen. Weight loss measurements were taken by continuous weighing of the test cup to the nearest 0.001 g with an electronic scale (Ohaus PA313, USA). Data were transferred to a computer. Weight loss was plotted over time and when steady state (straight line) was reached, 8 h more were registered. Thickness value was the mean value of five measurements and it was used for water vapour permeability calculations. The water vapour transmission rate (WVTR) was calculated from the slope (G) of a linear regression of weight loss versus time (Eq. (7)) and measured water vapour permeability (P) was calculated according to Eq. (8):

$$\mathrm{WVTR} = \frac{G}{A} \tag{7}$$

$$P = \mathrm{cte} \cdot \frac{\mathrm{WVTR} \cdot l}{(p_{wi} - p_{w0})} \tag{8}$$

where l is the film thickness; A is the film exposed area, p_{wo} is the partial pressure of water vapour at the film surface outside the cup, p_{wi} is the partial pressure of water vapour of distilled water or saturated solution inside the cup, and cte is a constant that satisfies unit conversions. Corrected values of water vapour permeability (P_c) were obtained according to the equation proposed by Gennadios, Weller, and Gooding (1994):

$$P_c = \mathrm{cte} \cdot \frac{\mathrm{WVTR} \cdot l}{\Delta P_r} \tag{9}$$

Δp_r is the difference of water vapour partial pressure at each side of the film. % Error was calculated as follows:

$$\%\ \mathrm{Error} = \frac{(P_c - P)}{P_c} \cdot 100 \tag{10}$$

The test was carried out in triplicate for each film.

2.12. Solubility and diffusivity of water in the film

The solubility coefficient of water in the film was determined through the first derivate of GAB model divided by the water vapour partial pressure, p_w, based on the experimental data of water sorption isotherm:

$$\beta = \frac{C \cdot k \cdot w_0}{p_w} \left\{ \frac{1}{(1 - k \cdot a_w) \cdot (1 - k \cdot a_w + C \cdot k \cdot a_w)} - \frac{a_w}{[(1 - k \cdot a_w) \cdot (1 - k \cdot a_w + C \cdot k \cdot a_w)]^2} \cdot [-k(1 - k \cdot a_w + C \cdot k \cdot a_w) + (1 - k \cdot a_w) \cdot (-k + C \cdot k)] \right\} \tag{11}$$

The permeability coefficient was calculated as the product of the solubility and diffusivity coefficients. The water diffusion coefficient was determined from P_c, β and ρ values. The β' value used to determine the diffusion coefficient, in each case, was the median of the a_w range used in the permeability measurement:

$$D_{eff} = \frac{P_c}{\beta' \cdot \rho} \tag{12}$$

2.13. Statistical analysis

Statistics on a completely randomized design were performed with the analysis of variance (ANOVA) procedure using Graph Pad Prism 5.01 software. Tukey's multiple range test ($p \leq 0.05$) was used to detect differences among mean values of films properties.

Table 1
Chemical composition of sugarcane bagasse and cellulose fibres.

	% Cellulose	% Hemicellulose	% Lignin
Sugarcane bagasse	40.3 ± 1.6	21.4 ± 1.6	23.84 ± 0.9
Alkali hydrolysis	68.1 ± 2.1	2.3 ± 0.7	8.93 ± 1.0
Bleaching	83.6 ± 1.6	0.87 ± 0.5	3.25 ± 0.7

3. Results and discussion

3.1. Characterization of CNC

The chemical composition of the sugarcane bagasse after each stage of the chemical treatment is shown in Table 1. It was found that, at the end of the alkaline treatment, the cellulose content increases while the hemicelluloses and lignin contents decrease significantly. This is due to the alkaline treatment of lignocellulosic fibres, the fibres surface area increases and causes the polysaccharides to become more susceptible to hydrolysis. Zuluaga et al. (2009) reported that by using $NaClO_2$, a greater removal of lignin was obtained. After the bleaching process, an increase in cellulose content and a decrease in lignin content were observed.

Fig. 1 shows micrographs obtained by SEM and TEM of CF, and CNC. After the extraction process, the fibres presented similar morphological structure to CF obtained by Zimmermann, Bordeanu, and Strub (2010). CF exhibited an irregular size with a diameter of approximately 10 μm. SEM of CNC (Fig. 1b) shows a crystal-like structure after the acid hydrolysis process. Average length (L) and diameter (D) of CNC and L/D values that were obtained from TEM images are 247.51 (±32.34), 10.11 (±3.36) and 24.48 nm, respectively (Fig. 1c). The L and D values present a typical Gaussian distribution.

X-ray diffractograms were performed on CF and CNC powder (Fig. 2). The diffractograms display a mixture of polymorphs of cellulose I (typical peaks at $2\theta \sim 15^\circ$ and 22°) and cellulose II (Klemm, Heublein, Fink, & Bohn, 2005). In order to determine the crystalline degree of the samples, the ratio of the crystalline area to the total area can be calculated. However, to determine the crystalline area, the amorphous part must be known. This can be obtained by X-ray diffraction of a completely amorphous cellulose sample (Bondeson et al., 2006). Nevertheless, by comparing the intensities of the diffraction peaks of both samples, it is possible to determine a change in crystallinity. The intensity of the peaks in the diffractogram of CNC was significantly higher than the peak intensities in the diffractogram of FC. Thus, the crystallinity increased as a result of the acid hydrolysis treatment. Results indicate that the amorphous regions were removed by the acid hydrolysis. Chen, Liu, Chang, Cao, and Anderson (2009) obtain similar results in pea hull fibres.

3.2. Scanning electron microscopy (SEM) of starch/CNC films

Fig. 3 shows a microphotograph obtained by SEM of starch/CNC films. Images indicate that CNC are homogeneously dispersed within the polymer matrix, thus, indicating that a good dispersion of nanoreinforcements was obtained.

3.3. Film solubility in water

Solubility in water is an important property of films for food packaging applications. Some potential uses may require water insolubility to enhance product integrity and water resistance. However, in other cases, water solubility of the film before

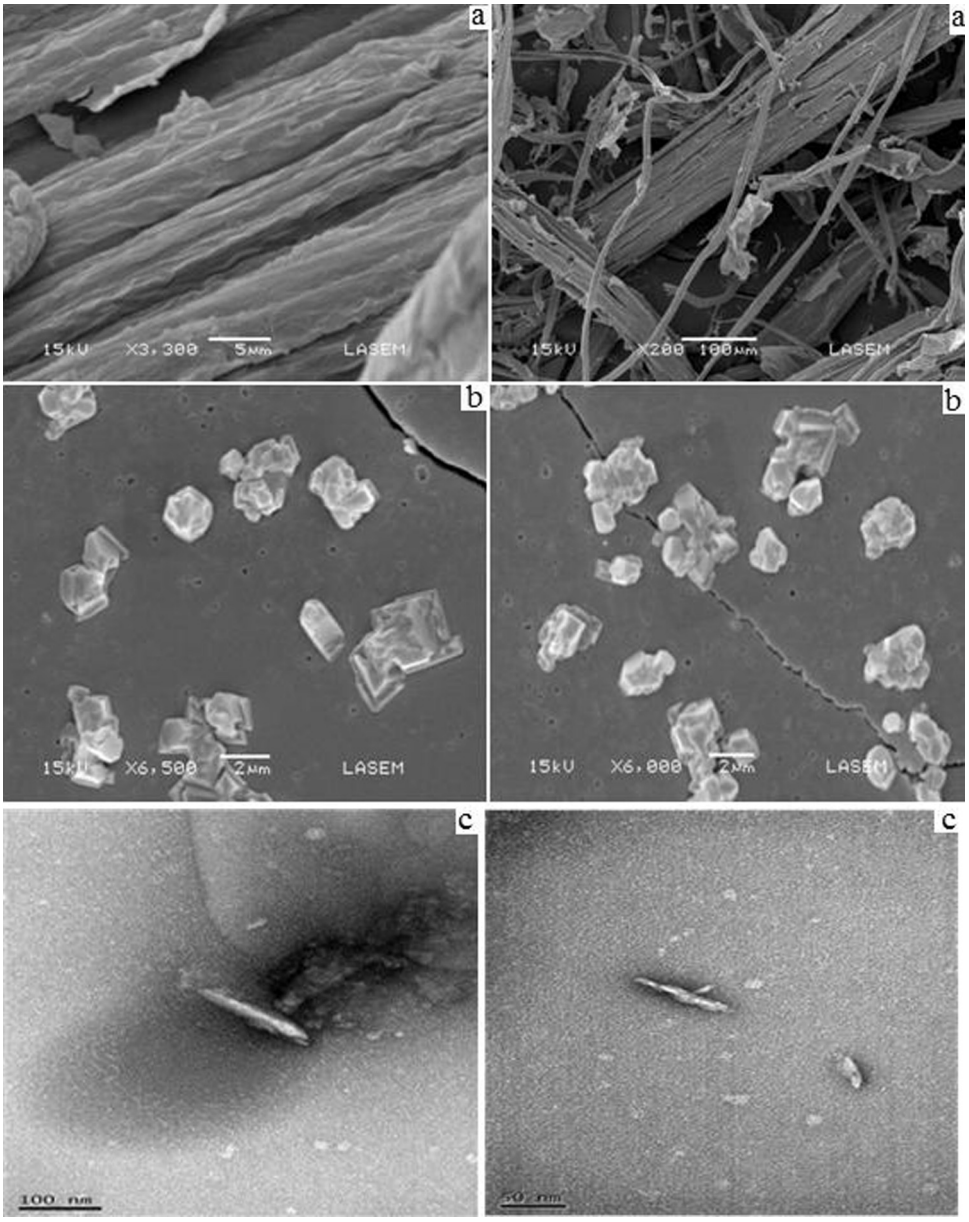

Fig. 1. SEM microphotographs of CF (a) and CNC (b). TEM images of CNC (c).

product consumption might be useful as in encapsulation of food or additives. The addition of CNC reduces the film solubility from 26.6% to 18.5% (Table 2). It is indicative of strong interactions between starch chains and CNC in the film matrix. CNC are capable of interacting with starch chains through hydrogen bonds with the hydroxyl groups of CNC. These interactions provide stability and resistance to starch/CNC films. Rhim and Ng (2007) reported that the reduction observed in solubility of films reinforced with different nanofillers is mainly related to the strong hydrogen bond formation between hydroxyl groups of the biopolymer and the nanoparticles. These results were corroborated by Abdollahi, Alboofetileh, Rezaei, and Behrooz (2013) in alginate/CNC films. Besides Tunc et al. (2007) informed that these interactions improve the cohesiveness of the biopolymer matrix and decrease the water sensitivity because water molecules are not able to break these strong bonds. Cao, Chen, Chang, Stumborg, and Huneault (2008) indicated that the matrix structure and the resulting competition between matrix/filler and filler/filler interactions are among the most important factors that determine the reinforcing effect of nanofillers.

Table 2
Physicochemical characterization of starch films and starch/CNC films.

	% Solubility	Contact angle	Surface energy ($mJ\,m^{-2}$)	Density ($g\,cm^{-3}$)	Mechanical properties		
					T (MPa)	ε (%)	Y (MPa)
Starch	26.6 ± 1.0	38.2 ± 1.3	59.5 ± 1.0	1.34 ± 0.07	2.8 ± 1.0	44.9 ± 1.6	112 ± 9
Starch/CNC	18.5 ± 1.3	96.3 ± 1.2	25.5 ± 1.1	1.36 ± 0.06	17.4 ± 1.4	9.1 ± 1.3	520 ± 12

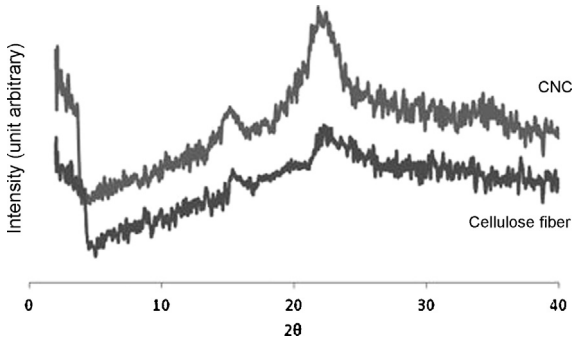

Fig. 2. X-ray diffraction of CF and CNC.

3.4. Surface hydrophobicity assay

Wettability of films can be obtained through contact angle measurements (θ) of a water drop on the film. An increase in the contact angle indicates an increase in film hydrophobicity. Table 2 shows that the contact angle and the surface energy were altered by CNC incorporation. These results, as well as the solubility values, indicate a strong interaction between starch chains and CNC. The formation of hydrogen bonds between them reduces the interaction between water and the film surface. According to Cao et al. (2008) the observed improvement in the hydrophobic character of films with CNC addition is mainly related to the highly hydrophobic properties of the nanocellulose crystals. Abdollahi et al. (2013) observed a high increment of the hydrophobic character in alginate films when they were added with CNC.

3.5. Mechanical properties

Fillers with a high ratio of the largest to the smallest dimension (i.e. aspect ratio) are particularly interesting because of their high specific surface area, providing better reinforcing effects (Azizi Samir et al., 2004). Table 2 shows the effect of CNC incorporation into starch films. An important increase in T and Y and a decrease in % ε were observed. The high T and Y values indicated that the filler was properly dispersed in the matrix structure. Similarities in the chemical structure of cellulose and starch promote strong interactions between them. The elongation at break decreases due to the rigid nature of the filler and it is in agreement with previous results published in the literature (Müller, Borges, & Yamashita, 2009; Pereda, Amica, Rácz, & Marcovich, 2011).

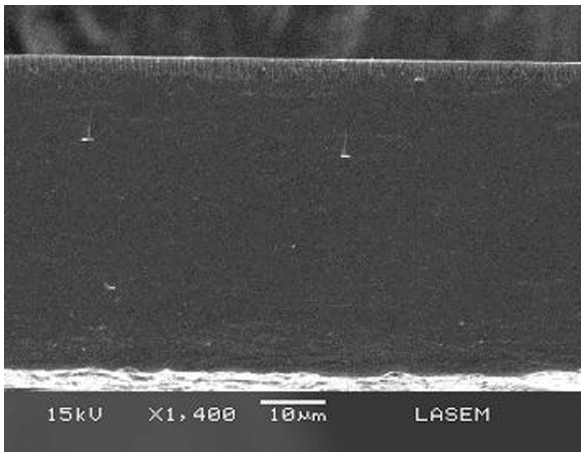

Fig. 3. SEM microphotograps of starch/CNC films.

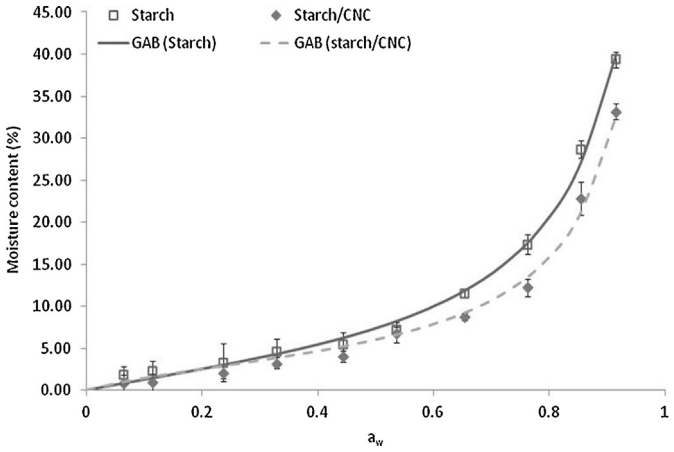

Fig. 4. Moisture sorption isotherm data of starch films (□) and starch/CNC films (♦) and GAB model fitting for starch films (—) and starch/CNC films (– –).

3.6. Density

Film density values show not significant differences between starch and starch/CNC films (Table 2). This could be due to the similarity between densities of both materials and the low proportion of the filler into the film matrix. Azizi Samir et al. (2004) reported that density of poly (oxyethylene) was not affected by the reinforcement with cellulose nanocrystals.

3.7. Moisture sorption isotherm

Fig. 4 shows moisture sorption isotherm data obtained at 25 °C for starch and starch/CNC films. Sorption curves were typical of water sensitive polymers and sorption levels were within the range reported for starch film (Kampeerapappun, Aht-ong, Pentrakoon, & Srikulkit, 2007; Müller, Laurindo, & Yamashita, 2011). Experimental data present similar values at low a_w range for starch and starch/CNC films and take an exponential course at high relative humidities (above 0.60). Under these conditions, hydrophilic polymeric chains swell altering its structure. Experimental data obtained for starch/CNC film indicate that incorporation of CNC reduces water sorption, demonstrating that water has less affinity for the film.

Sorption data corroborate the behaviour observed in solubility tests and contact angle measurements. CNC present stronger interaction with starch than with water. The number of active sites for water binding decreases due to the formation of strong bonds between starch and CNC, reducing the moisture content of starch/CNC films as water activity increases. This effect is more evident in the medium water activity range. Pereda et al. (2011) indicated that due to the strong interaction between starch and CNC, the plasticizer plays a determining role in the sorption process. The material plasticization generates a greater opening to new water adsorption sites, yielding higher moisture content in the film. Glycerol incorporated into the film formulation produces the plasticization of the polymeric structure which leads to an exponential increase in the moisture content of the film. Kristo and Biliaderis (2007) and George (2012) obtained similar sorption isotherms of starch films with the addition of starch nanocrystals and gelatine film with the addition of CNC, respectively.

Table 3 shows the GAB model parameters obtained for starch films and starch/CNC films. The water monolayer value decreases with incorporation of CNC into polymeric matrix. This indicates that CNC reduce the site number where water molecules can interact with starch chains, decreasing the adsorption of water in the film. Bilbao-Sainz, Bras, Williams, Sénechal, and Orts (2011) obtained

Table 3
Estimated GAB parameters for starch films and starch/CNC films.

	w_0	C	k	R^2	% Error
Starch	5.657	2.421	0.9474	0.9917	1.13
Starch/CNC	3.813	4.580	0.9688	0.9853	1.49

a decrease in monolayer values of HPMC films with increasing CNC content. A similar behaviour was observed for high amylose starch based films, indicating that water acts as a strong solvent or swelling agent for the polymer (Bertuzzi et al., 2003).

3.8. Water vapour permeability, solubility and diffusivity

Fig. 5 shows the water solubility coefficients as a function of water activity for starch films and starch/CNC films. At low values of a_w, solubility remains practically constant, but there is an exponential increase from $a_w = 0.6$, for both kind of films. This inflexion point corresponds to the completion of the monolayer as can be seen in Table 3. Beyond $a_w = 0.6$, water molecules recover mobility and the water solubility in the film increases notoriously. In the range of $a_w = 0.55–0.85$, the differences between solubility of starch films and starch/CNC films are the greatest, showing the effect of CNC incorporation in the starch matrix. CNC act delaying the plasticizing effect of water on film due to the high interaction between OH-groups of starch and CNC. At high values of a_w, the solubility values of both films merge.

Table 4 shows corrected and uncorrected water vapour permeability for the different ranges of a_w used to generate the water vapour gradient through the film. The % Error was calculated according to the procedure delineated by Gennadios et al. (1994). The results indicate that, at the same value of Δa_w, the % Error in the permeability measurements presented by starch films increases with a_w at each side of the film. However, in the case of starch/CNC films, % Error remains practically constant. This is due to the difference between WVTR of both films and indicates the importance of data correction to obtain a better understanding of barrier properties of these films. According to Gennadios et al. (1994) the higher the WVTR through a film the more important is air gap resistance and the larger the error produced from overlooking this effect. The % Error observed for starch/CNC films are lower than that obtained for starch films due to the low WVTR of the nanocomposites films. Permeability increases with a_w at each side of the film when similar driving force (Δa_w) was used in starch film. However, in contrast to results reported by Slavutsky and Bertuzzi (2012) about starch/MMT films, water permeability of starch/CNC film was not dependent on a_w. This would indicate that the permeation process is controlled by the diffusion of water through the film and not by the solubility of water in the matrix. According to Kristo and Biliaderis (2007), the addition of rigid crystalline structures produces a tortuous path that hinders the passage of water molecules through the film matrix. The driving force and the a_w at each side of the film play important roles in the permeability process. At high a_w, adsorption of water molecules produces a great increment on mobility of starch chain in the starch film, but it is less important in starch/CNC films.

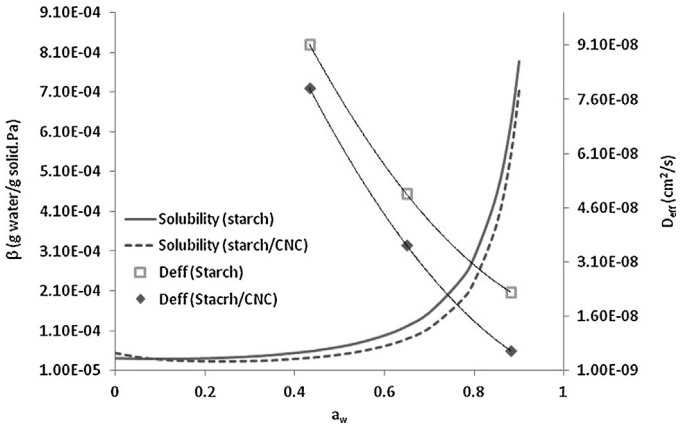

Fig. 5. Water solubility coefficient of starch films (—) and starch/CNC films (– –) and diffusion coefficient of starch films (□) and starch/CNC films (♦) as function of a_w.

Diffusion coefficient data provide more information and evidence of CNC effect in the water barrier behaviour of the starch matrix. In general, at low values of a_w, when moisture content increases, the films swell and increase their plasticization, therefore diffusivity increases significantly (Slavutsky & Bertuzzi, 2012). Nevertheless, when a_w are higher than 0.5, diffusivity decreases. In this work, the phenomenological analysis was performed at high water content. Table 4 shows solubility and diffusivity coefficients obtained by application of Eqs. (11) and (12), respectively. Obtained values indicate that incorporation of CNC reduces the D_{eff} of starch film. At a similar driving force ($\Delta a_w = 0.2$), D_{eff} decreases with the increment of a_w values at each side of the film. It can be explained by the fact that water molecules plasticize the film, generate the polymer matrix relaxation, and promote the adsorption of water molecules in new active sites. Water molecule clustering occurs, resulting in a decrease of diffusivity.

When the driving force is 0.2 and a_w at each side of the film are lower than 0.5, there is a little difference between solubility of starch films and starch/CNC films. In this range, the permeation process is controlled by the diffusion process. SEM images indicated that CNC are homogenously dispersed into the starch matrix. Several authors have reported that CNC incorporation produces a tortuous pathway that decreases D_{eff} (Azizi Samir et al., 2004; Cao et al., 2008; George, 2012). A combined effect of solubility and diffusivity on permeability is found at a_w middle values. It is originated by the tortuous pathway and the lower adsorption of water molecules in the starch/CNC matrix. In this zone, the plasticizing effect of water is more important on the starch matrix. The homogeneous dispersion of CNC into starch matrix provides an effective tortuous pathway, producing a less favourable diffusion of water molecules, making the water permeability more dependent on D_{eff}.

Fig. 5 shows D_{eff} vs. a_w when the driving force is equal 0.2. The variation of diffusivity and solubility coefficients with a_w, and the differences between both films tested can be observed. According to Debeaufort, Voilley, and Meares (1994), this kind of behaviour may be explained by the water cluster formation. Once a monolayer of water molecules moistens the film, a further increase in moisture results in "free water" that does not interact with the polymer. The free water molecules aggregate to form di-, tri-, and tetramer clusters. The molecular volume of these clusters is larger than that of monomers and results in decreased diffusion. The incorporation of CNC maintains the effect on water diffusivity at high a_w values due to the generation of a tortuous pathway that provides an extra decrease of D_{eff}.

In addition, Wan et al. (2009) indicated that the resulting interaction between starch and glycerol may promote adsorption of moisture, due to dimensional changes in the area where the adhesion between interfaces (starch–glycerol) is poor, thus creating a step that facilitates the accumulation of water molecules. However, due to the chemical similarity between starch and CNC, structural and interface defects decrease, creating a strong resistance to the passage of water molecules. It could be conclude that due to the increase in the plasticization process that occurs in the polymer structure, permeation process depends mainly on the diffusion coefficient and on the formation of a tortuous path by CNC, which at high moisture contents still produces a barrier effect on water molecule movement. This arises from the results observed in

Table 4
Phenomenological coefficients of starch films and CNC/starch films.

$a_w^{ext} - a_w^{int}$	$\|\Delta a_w\|$	P (g/m s Pa)	P_c (g/m s Pa)	Error (%)	β' (g_w/g_{ds} Pa)	D_{eff} (cm^2/s)
Starch						
0.329–0.536	0.207	3.73E−10	7.13E−10	47.64	5.83E−05	9.13E−08
0.536–0.762	0.226	4.59E−10	8.02E−10	42.81	1.20E−04	4.98E−08
0.762–1.000	0.238	6.93E−10	18.7E−10	63.13	6.19E−04	2.27E−08
0.329–0.762	0.433	3.28E−10	5.03E−10	34.79	8.05E−05	4.66E−08
0.000–1.000	1	6.28E−10	9.08E−10	33.30	6.99E−05	9.70E−08
Starch/CNC						
0.329–0.536	0.207	2.73E−10	4.45E−10	38.55	4.13E−05	7.92E−08
0.536–0.762	0.226	2.67E−10	4.26E−10	37.35	8.79E−05	3.57E−08
0.762–1.000	0.238	2.80E−10	4.72E−10	42.81	5.40E−04	6.43E−09
0.329–0.762	0.433	2.65E−10	4.21E−10	36.98	5.75E−05	5.38E−08
0.000–1.000	1	2.28E−10	3.33E−10	31.46	4.96E−05	4.94E−08

Δa_w = 0.762–1.00 range, where the decrease in D_{eff} due to the CNC incorporation was of approximately 74%, whereas in the rest of the ranges studied, the decrease was about 35%.

4. Conclusions

CNC was prepared from CF obtained by alkaline hydrolysis of sugarcane bagasse. The incorporation of CNC into the starch films matrix improved their water resistance and water barrier properties. The similar chemical structures of the polymer matrix and the CNC led to strong adhesion between them through hydrogen bonding. Contac angle measurements and water sorption isotherms indicated that reinforced films have less affinity by water molecules. Permeability, diffusivity and solubility coefficients indicated that the permeation process was controlled by the water diffusion and was depend on the tortuous pathway formed by CNC incorporation. The decrease in surface hydrophilicity and the improvement in water vapour barrier properties with the addition of CNC showed that these nanocomposites present excellent potential as a new biomaterial for application in food packaging and conservation.

Acknowledgements

The financial support provided by CIUNSa (Proyecto N° 1895/2) and by ANPCyT (IP-RPH 2007) are gratefully acknowledged. The authors thank technical assistance of LASEM (Laboratorio de Microscopia Electrónica de Barrido, ANPCyT, CONICET, UNSa).

References

Abdollahi, M., Alboofetileh, M., Rezaei, M., & Behrooz, R. (2013). Comparing physico-mechanical and thermal properties of alginate nanocomposite films reinforced with organic and/or inorganic nanofillers. *Food Hydrocolloids*, *32*(2), 416–424.
Al-Muhtaseb, A. H., McMinn, W. A. M., & Magee, T. R. A. (2002). Moisture sorption isotherm characteristics of food products: A review. *Food and Bioproducts Processing*, *80*(2), 118–128.
ASTM. (2000a). *E96. Standard test methods for water vapor transmission of materials*. Philadelphia: Standards American Society for Testing and Materials.
ASTM. (2000b). *D882. Standard test methods for tensile properties of thin plastic sheeting*. Philadelphia: Standards American Society for Testing and Materials.
Azeredo, H. M. C. D. (2009). Nanocomposites for food packaging applications. *Food Research International*, *42*(9), 1240–1253.
Azizi Samir, M. A. S., Alloin, F., Sanchez, J.-Y., & Dufresne, A. (2004). Cellulose nanocrystals reinforced poly(oxyethylene). *Polymer*, *45*(12), 4149–4157.
Belbekhouche, S., Bras, J., Siqueira, G., Chappey, C., Lebrun, L., Khelifi, B., et al. (2011). Water sorption behavior and gas barrier properties of cellulose whiskers and microfibrils films. *Carbohydrate Polymers*, *83*(4), 1740–1748.
Bertuzzi, M. A., Armada, M., & Gottifredi, J. C. (2003). Thermodynamic analysis of water vapour sorption of edible starch based films. *Food Science and Technology International*, *9*(2), 115–121.
Bertuzzi, M. A., Castro Vidaurre, E. F., Armada, M., & Gottifredi, J. C. (2007). Water vapor permeability of edible starch based films. *Journal of Food Engineering*, *80*(3), 972–978.
Bilbao-Sainz, C., Bras, J., Williams, T., Sénechal, T., & Orts, W. (2011). HPMC reinforced with different cellulose nano-particles. *Carbohydrate Polymers*, *86*(4), 1549–1557.
Bondeson, D., Mathew, A., & Oksman, K. (2006). Optimization of the isolation of nanocrystals from microcrystalline cellulose by acid hydrolysis. *Cellulose*, *13*, 171–180.
Bondeson, D., & Oksman, K. (2007). Polylactic acid/cellulose whisker nanocomposites modified by polyvinyl alcohol. *Processing*, *38*, 2486–2492.
Cao, X., Chen, Y., Chang, P. R., Stumborg, M., & Huneault, M. A. (2008). Green composites reinforced with hemp nanocrystals in plasticized starch. *Journal of Applied Polymer Science*, *109*, 3804–3810.
Chen, Y., Liu, C., Chang, P. R., Cao, X., & Anderson, D. P. (2009). Bionanocomposites based on pea starch and cellulose nanowhiskers hydrolyzed from pea hull fibre: Effect of hydrolysis time. *Carbohydrate Polymers*, *76*(4), 607–615.
Debeaufort, F., Voilley, A., & Meares, P. (1994). Water vapour permeability and diffusivity through methylcellulose edible films. *Journal of Membrane Science*, *91*, 125–133.
Dujardin, E., Blaseby, M., & Mann, S. (2003). Synthesis of mesoporous silica by sol–gel mineralisation of cellulose nanorod nematic suspensions. *Journal of Materials Chemistry*, *13*(4), 696–699.
Gennadios, A., Weller, C. L., & Gooding, C. H. (1994). Measurement errors in water vapor permeability of highly permeable, hydrophilic edible films. *Journal of Food Engineering*, *21*(4), 395–409.
Geoering, H. K., & Van Soest, P. J. (1970). Forage fiber analysis. Apparatus, reagents, procedure and some applications. In *Agriculture handbook 379*. Washington DC: ARS. USDA.
George, J. (2012). High performance edible nanocomposite films containing bacterial cellulose nanocrystals. *Carbohydrate Polymers*, *87*(3), 2031–2037.
Helbert, W., Cavaillé, C. Y., & Dufresne, A. (1996). Thermoplastic nanocomposites filled with wheat straw cellulose whiskers. Part I: Processing and mechanical behaviour. *Polymer Composites*, *17*(4), 604–611.
Kampeerapappun, P., Aht-ong, D., Pentrakoon, D., & Srikulkit, K. (2007). Preparation of cassava starch/montmorillonite composite film. *Carbohydrate Polymers*, *67*(2), 155–163.
Kester, J. J., & Fennema, O. R. (1986). Edible films and coatings: A review. *Food Science and Technology*, *40*(12), 47–59.
Klemm, D., Heublein, B., Fink, H. P., & Bohn, A. (2005). Cellulose: Fascinating biopolymer and sustainable raw material. *Angewandte Chemie International Edition*, *44*, 3358–3393.
Kristo, E., & Biliaderis, C. (2007). Physical properties of starch nanocrystal-reinforced pullulan films. *Carbohydrate Polymers*, *68*(1), 146–158.
Kvien, I., Sugiyama, J., Votrubec, M., & Oksman, K. (2007). Characterization of starch based nanocomposites. *Journal of Materials Science*, *42*(19), 8163–8171.
Kwok, D. Y., & Neumann, A. W. (1999). Contact angle measurement and contact angle interpretation. *Advances in Colloid and Interface Science*, *81*, 167–249.
Larotonda, F. D. S., Matsui, K. N., Sobral, P. J. A., & Laurindo, J. B. (2005). Hygroscopicity and water vapor permeability of Kraft paper impregnated with starch acetate. *Journal of Food and Engineering*, *71*, 394–402.
Lima, M. M. D., & Borsali, R. (2004). Rodlike cellulose microcrystals: Structure, properties, and applications. *Macromolecular Rapid Communications*, *25*(7), 771–787.
Müller, C. M. O., Borges, J., & Yamashita, F. (2009). Effect of cellulose fibers on the crystallinity and mechanical properties of starch-based films at different relative humidity values. *Carbohydrate Polymers*, *77*(2), 293–299.
Müller, C. M. O., Laurindo, J. B., & Yamashita, F. (2011). Effect of nanoclay incorporation method on mechanical and water vapor barrier properties of starch-based films. *Industrial Crops and Products*, *33*(3), 605–610.
Müller, C. M. O., Yamashita, F., & Borges Laurindo, J. (2008). Evaluation of the effects of glycerol and sorbitol concentration and water activity on the water barrier properties of cassava starch films through a solubility approach. *Carbohydrate Polymers*, *72*, 82–87.
Oksman, K., Mathew, A. P., Bondeson, D., & Kvien, I. (2006). Science and Manufacturing process of cellulose whiskers/polylactic acid nanocomposites. *Composites Science and Technology*, *66*, 2776–2784.
Paralikar, S. A., Simonsen, J., & Lombardi, J. (2008). Poly(vinyl alcohol)/cellulose nanocrystal barrier membranes. *Journal of Membrane Science*, *320*, 248–258.

Pereda, M., Amica, G., Rácz, I., & Marcovich, N. E. (2011). Structure and properties of nanocomposite films based on sodium caseinate and nanocellulose fibers. *Journal of Food Engineering*, *103*(1), 76–83.

Podsiadlo, P., Choi, S. Y., Shim, B., Lee, J., Cuddihy, M., & Kotov, N. A. (2005). Molecularly engineered nanocomposites: Layer-by-layer assembly of cellulose nanocrystals. *Biomacromolecules*, *6*, 2914–2918.

Rhim, J. W., & Ng, P. K. W. (2007). Natural biopolymer-based nanocomposite films for packaging applications. *Critical Reviews in Food Science and Nutrition*, *47*, 411–433.

Savadekar, N. R., & Mhaske, S. T. (2012). Synthesis of nano cellulose fibers and effect on thermoplastics starch based films. *Carbohydrate Polymers*, *89*(1), 146–151.

Slavutsky, A. M., & Bertuzzi, M. A. (2012). A phenomenological and thermodynamic study of the water permeation process in corn starch/MMT films. *Carbohydrate Polymers*, *90*(1), 551–557.

Spiess, W. E. L., & Wolf, W. F. (1983). The results of the COST 90 project on water activity. In *Physical properties of foods*. London: Applied Science Publishers.

Svagan, A. J., Hedenqvist, M. S., & Berglund, L. (2009). Reduced water vapour sorption in cellulose nanocomposites with starch matrix. *Composites Science and Technology*, *69*(3–4), 500–506.

Tashiro, K., & Kobayashi, M. (1991). Theoretical evaluation of three-dimensional elastic constants of native and regenerated celluloses: Role of hydrogen bonds. *Polymer*, *32*, 1516–1526.

Tunc, S., Angellier, H., Cahyana, Y., Chalier, P., Gontard, N., & Gastaldi, E. (2007). Functional properties of wheat gluten/montmorillonite nanocomposite films processed by casting. *Journal of Membrane Science*, *289*(1), 159–168.

Wan, Y. Z., Luo, H., He, F., Liang, H., Huang, Y., & Li, X. L. (2009). Mechanical, moisture absorption, and biodegradation behaviours of bacterial cellulose fibre-reinforced starch biocomposites. *Composites Science and Technology*, *69*(7–8), 1212–1217.

Wang, B., & Sain, M. (2007). Science and Isolation of nanofibers from soybean source and their reinforcing capability on synthetic polymers. *Composites Science and Technology*, *67*, 2521–2527.

Wiles, J. L., Vergano, P. J., Barron, F. H., Bunn, J. M., & Testin, R. F. (2000). Water vapor transmission rates and sorption behavior of chitosan films. *Food Engineering and Physical Properties*, *65*(7), 1175–1179.

Zanin, G. M., Santana, C. C., Bon, E. P. S., Giordano, R. C. L., de Moraes, F. F., & Andrietta, S. R. (2000). Brazilian bioethanol program. *Applied Biochemistry and Biotechnology*, *84–86*(1–9), 1147–1161.

Zimmermann, T., Bordeanu, N., & Strub, E. (2010). Properties of nanofibrillated cellulose from different raw materials and its reinforcement potential. *Carbohydrate Polymers*, *79*(4), 1086–1093.

Zuluaga, R., Luc, J., Cruz, J., Vélez, J., Mondragon, I., & Gañán, P. (2009). Cellulose microfibrils from banana rachis: Effect of alkaline treatments on structural and morphological features. *Carbohydrate Polymers*, *76*(1), 51–59.